IET Generation, Transmission & Distribution

Research Article

IET Journals
The Institution of Engineering and Technology

High-fidelity large-signal order reduction approach for composite load model

ISSN 1751-8687
Received on 18th May 2020
Revised 13th July 2020
Accepted on 29th July 2020
doi: 10.1049/iet-gtd.2020.0972
www.ietdl.org

Zixiao Ma[1] ✉, Zhaoyu Wang[1], Dongbo Zhao[2], Bai Cui[3]

[1]*Department of Electrical and Computer Engineering, Iowa State University, Ames, IA 50011, USA*
[2]*Argonne National Laboratory, Argonne, IL 60439, USA*
[3]*National Renewable Energy Laboratory, Golden, CO 80401, USA*
✉ *E-mail: zma@iastate.edu*

Abstract: With the increasing penetration of electronic loads and distributed energy resources, conventional load models cannot capture their dynamics. Therefore, a new comprehensive composite load model is developed by Western Electricity Coordinating Council (WECC). However, this model is a complex high-order non-linear system with multi-time-scale property, which poses challenges on power system studies with heavy computational burden. In order to reduce the model complexity, the authors firstly develop a large-signal order reduction (LSOR) method using singular perturbation theory. In this method, the fast dynamics are integrated into the slow ones to preserve transient characteristics of the former. Then, accuracy assessment conditions are proposed and embedded into the LSOR to improve and guarantee the accuracy of reduced-order model. Finally, the reduced-order WECC composite load model is derived by using the proposed algorithm. Simulation results show that the reduced-order large-signal model significantly alleviates the computational burden while maintaining similar dynamic responses as the original composite load model.

1 Introduction

Power system load modelling is important for power system studies such as stability analysis, optimisation, and controller design [1]. Although this topic has been widely studied, it is still a challenging problem due to increasing diversity of load components and lack of detailed load information and measurements.

Load models can be classified into static and dynamic ones. Static load models such as static constant impedance–current–power (ZIP) model and exponential model have simple model structures [2, 3]. However, they cannot capture the dynamic load behaviours [4–10]. Motivated by the 1996 blackout of the Western Systems Coordinating Council, a widely-used dynamic composite load model was developed [11]. The model consists of a ZIP and a dynamic induction motor (IM). It was designed to represent highly stressed loading conditions in summer peak hours. However, this interim load model was unable to capture the fault-induced delayed voltage recovery events [7]. A preliminary Western Electricity Coordinating Council (WECC) composite load model was proposed by adding an impedance representing the electrical distance between substation and end-users, an electronic load, and a single-phase motor [12–14]. After a series of improvements, the latest WECC composite load model (CMPLDWG) is developed as shown in Fig. 1. The electrical distance between the substation and end-users is represented by a substation transformer, a shunt reactance, and a feeder equivalent. The model consists of three

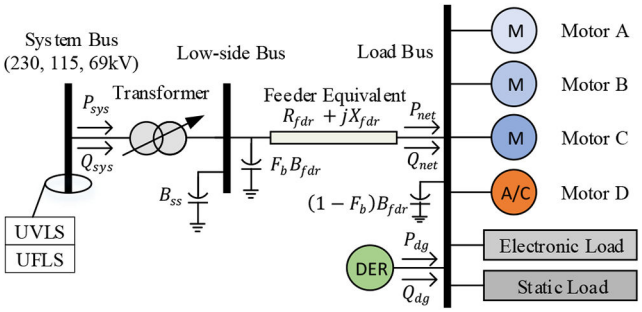

Fig. 1 *Schematic diagram of the WECC CMPLDWG [13]*

three-phase motors, one aggregate single-phase AC motor, one static load, one power electronics component, and one distributed energy resource (DER). The DER in CMPLDWG is currently represented by the PVD1 model [15]. However, PVD1 has 5 modules, 121 parameters, and 16 states, which is as complex as the CMPLDW itself. Therefore, the Electric Power Research Institute (EPRI) has developed a simpler yet more comprehensive model to replace PVD1, which is named as DER_A model [15].

The above WECC CMPLDW + DER_A model is a *complex high-order non-linear* dynamical system with *multi-time-scale* property, which means the state vector is high-dimensional and the transient velocity of each state varies significantly. These characteristics result in two main challenges. Firstly, it increases the difficulty of dynamic stability analysis due to the numerous state variables. Secondly, it makes simulation studies of a high-order power system computationally demanding or even infeasible. There are two main reasons for this high computational burden. One reason is the shear dimensionality of the problem. The other comes from the two-time-scale property of the model. This makes solving the model a stiff ordinary differential equation (ODE) problem, which requires small time steps to calculate the fast dynamics, and consequently results in long computational time to capture slow dynamics. The fast dynamics are often introduced by the intentionally added inductance and capacitance, moment of inertia, and parasitic elements inherent in the system [16]. However, simply neglecting the fast dynamics may lead to modelling inaccuracies in dynamic response and stability property. In order to accelerate computation while maintaining the accuracy and faithful stability property of the original load model, it is imperative to develop a high-fidelity reduced-order load model. To our best knowledge, this is the first paper on dynamic order reduction of WECC composite load model especially containing the DER_A model.

The existing model reduction methods usually project the higher dimensional counterpart into a lower dimensional subspace where dynamic features of the original model dominate. Singular perturbation is the kind of method which considers the fast dynamics as boundary-layers and includes their solutions into slow dynamics. Singular perturbation method is suitable for analysing two-time-scale problems and is widely used in power systems analysis. Previous applications include the derivation of reduced-

order modelling of synchronous machines [17], microgrids [18], and distribution grid-tied systems with wind turbines [19]. However, these papers fall short of guaranteed accuracy and cannot be directly applied to the WECC composite load model due to the different system characteristics.

Therefore, this paper develops a novel accuracy assessment theorem which takes into account the impact of external inputs on the accuracy of reduced system. By embedding the theorem, we propose a high-fidelity order reduction approach for WECC composite load model. The derived high-fidelity reduced-order model can replace the original model in power system simulations for stability analysis and control applications with less computational complexity. Specifically, we improve the accuracy from two aspects. Firstly, without any simplification or linearisation, we adopt the large-signal order reduction (LSOR) method based on singular perturbation theory to maintain all the dynamic characteristics of the original system. Secondly, we propose sufficient conditions for accurate order reduction, and then integrate them into the LSOR method to theoretically guarantee the high accuracy of the reduced-order model. Note that this proposed approach is general and can be applied to various dynamic models.

The rest of the paper is organised as follows. Section 2 proposes high-fidelity order reduction approach in a general form. Section 3 introduces mathematical representation of WECC composite load model. Section 4 derives the reduced-order model using the proposed method. Section 5 shows the simulation results and analysis. Section 6 concludes the paper.

2 High-fidelity order reduction method

Accurate load modelling is essential to power system studies. To solve the challenges raised by high-order characteristics of WECC composite load model, we propose a general approach for high-fidelity order reduction in this section. We first introduce the LSOR method based on singular perturbation theory. A novel accuracy assessment theorem is then derived and embedded into the LSOR to guarantee the accuracy of reduced-order model.

2.1 LSOR based on singular perturbation theory

Q1 Consider a standard singular perturbation model as follows:

$$\dot{x} = f(\boldsymbol{x}, \boldsymbol{z}, \boldsymbol{u}, \varepsilon), \tag{1}$$

$$\varepsilon\dot{z} = g(\boldsymbol{x}, \boldsymbol{z}, \boldsymbol{u}, \varepsilon), \tag{2}$$

where $\boldsymbol{x} \in \mathbb{R}^n$ represents slow state vector, $\boldsymbol{z} \in \mathbb{R}^m$ denotes fast state vector, $\boldsymbol{u} \in \mathbb{R}^p$ denote external input vector, and $\varepsilon \in [0, \varepsilon_0]$; f and g are Lipschitz continuous functions.

Remark 1: Selecting the perturbation coefficient ε for real physical systems is challenging. In most cases, we pick it based on our knowledge of the real system. In cases where it is unclear which parameter is small, we can locally linearise the system around the equilibrium point and use modal decomposition to identify the slow and fast dynamics.

When ε is small, the fast transient velocity $\dot{z} = g/\varepsilon$ can be much larger than that of the slow transient $\dot{x}$. To solve this two-time-scale problem, we can set $\varepsilon = 0$, then (2) degenerates to the following algebraic equation:

$$0 = g(\boldsymbol{x}, \boldsymbol{z}, \boldsymbol{u}, 0)\,. \tag{3}$$

Assuming that (3) has at least one isolated real root, and satisfies the implicit function theorem, then for each argument, we can obtain the quasi-steady-state (QSS) solution in a local vicinity around the isolated root

$$z = h(\boldsymbol{x}, \boldsymbol{u})\,. \tag{4}$$

Substituting (4) into (1) and setting $\varepsilon = 0$, we obtain the QSS model

$$\dot{x} = f(\boldsymbol{x}, h(\boldsymbol{x}, \boldsymbol{u}), \boldsymbol{u}, 0)\,. \tag{5}$$

We call the QSS system (5) the reduced-order model since its order drops from $n + m$ to n. The slow states can be obtained by solving the reduced-order model (5), whereas the fast states are represented by (4). However, (4) only gives approximate solution unless ε is zero. To quantify the error between approximate and actual fast states, we denote the error as $y = z - h(\boldsymbol{x}, \boldsymbol{u})$. Then in the fast-time-scale $\tau = t/\varepsilon$, the dynamics of y are governed as follows:

$$\begin{aligned}\frac{\mathrm{d}y}{\mathrm{d}\tau} &= G(\boldsymbol{x}, y, \boldsymbol{u}, \varepsilon)\\ &= g(\boldsymbol{x}, h(\boldsymbol{x}, \boldsymbol{u}) + y, \boldsymbol{u}, \varepsilon)\\ &\quad -\varepsilon\left[\frac{\partial h}{\partial x} f(\boldsymbol{x}, h(\boldsymbol{x}, \boldsymbol{u}) + y, \boldsymbol{u}, \varepsilon) + \frac{\partial h}{\partial u}\dot{u}\right].\end{aligned} \tag{6}$$

Let $\varepsilon = 0$, we obtain the boundary-layer model

$$\frac{\mathrm{d}y}{\mathrm{d}\tau} = g(\boldsymbol{x}, y + h(\boldsymbol{x}, \boldsymbol{u}), \boldsymbol{u}, 0)\,. \tag{7}$$

Note that the exact fast states are $\boldsymbol{z} = y + h(\boldsymbol{x}, \boldsymbol{u})$, but we do not know $(\boldsymbol{x}, y)$. Therefore, if we can guarantee the accuracy of reduced-order model and boundary-layer model, then we can use their solutions $(\hat{x}, \hat{y})$ instead of $(\boldsymbol{x}, y)$. However, these models are exact only when ε is exactly zero, which is obviously not the case for the studied system. Thus, we need to quantitatively assess the accuracy of reduced-order model when ε is small yet non-zero. This motivates the next subsection.

2.2 High-fidelity LSOR with accuracy assessment

Before deriving the performance guarantee of the proposed high-fidelity order reduction approach, we first introduce a few technical definitions and assumptions.

Definition 1: Class $\mathcal{K}$ function $\alpha: [0, t) \to [0, \infty)$ is a continuous strictly increasing function with $\alpha(0) = 0$.

Definition 2: Class $\mathcal{KL}$ function $\beta: [0, t) \times [0, \infty) \to [0, \infty)$ is a continuous function satisfying: for each fixed s, the function $\beta(r, s)$ belongs to class $\mathcal{K}$; for each fixed r, the function $\beta(r, s)$ is decreasing with respect to s and $\beta(r, s) \to 0$ for $s \to \infty$.

Definition 3: $|f| = O(\varepsilon)$ is equivalent to $|f| \leqslant k\varepsilon$.

Assumption 1: The functions f, g, and their first partial derivatives are continuous and bounded with respect to $(\boldsymbol{x}, \boldsymbol{z}, \boldsymbol{u}, \varepsilon)$; h and its first partial derivatives $\partial h/\partial x$, $\partial h/\partial u$ are locally Lipschitz; and the Jacobian $\partial g/\partial z$ has bounded first partial derivatives with respect to its arguments.

Assumption 2: The reduced-order model (5) is input-to-state stable with Lyapunov gain α as follows:

$$\hat{x} \leqslant \beta(\,\|\, x(0) \,\|\,, t) + \alpha(\,\|\, u \,\|\,), \tag{8}$$

where $\hat{x}$ is a solution of (5), β is a function of class $\mathcal{KL}$, α is a class $\mathcal{K}$ function, and $\|\cdot\|$ denotes any p-norm.

Assumption 3: The origin of the boundary-layer model (7) is a uniformly globally exponentially stable equilibrium and the solution $\hat{y}$ of (7) follows that

$$\|\, \hat{y}(\tau) \,\| \leqslant k_1 \mathrm{e}^{-a\tau},\ \forall\, \tau \geqslant 0, \tag{9}$$

where k_1 and a are positive constants.

Assumption 1 describes the basic growth conditions on the original system which are commonly satisfied for power load models. Assumptions 2 and 3 are stability conditions on reduced-order model and boundary-layer model, respectively.

Then, we propose the accuracy assessment index in the following accuracy assessment theorem, which will be embedded into the LSOR to realise high-fidelity order reduction. Before that, we give the following lemma for the proof of the theorem.

Lemma 1: Assume $\max\{\| x(0)\|, \| y(0)\|, \| u\|, \| \dot{u}\|\} \leqslant \mu$ holds for some positive constant μ. Then there exists a class $\mathscr{KL}$ function β_x, a class $\mathscr{K}$ function α_x and positive constants μ_x and ξ satisfying $\mu_x > \beta_x(\mu, 0) + \alpha_x(\mu) + \xi$ such that $\| x(t)\| \leqslant \mu_x$ for all $t \in [0, \infty)$.

Proof: According to the definition of class $\mathscr{KL}$ functions, we have $\beta_x(\mu, 0) \leqslant \mu, \forall\, \mu \in \mathbb{R}$, so $\mu_x > \mu$. Since x is continuous with finite initial conditions, we can find a maximal interval $[0, t_{\max})$, in which $\| x(t)\| \leqslant \mu_x$, where $t_{\max} > 0$ is defined as the upper bound of the interval. From the definition of μ and the assumption that $t_{\max}$ is finite, there must be some positive constant Δt such that $\| x(t)\| \leqslant \mu_x$ holds for all $t \in [0, t_{\max} + \Delta t)$. This contradicts that $t_{\max}$ is the upper bound, so $t_{\max}$ should be infinite and $\| x(t)\| \leqslant \mu_x, \forall\, t \in [0, \infty)$. □

Theorem 1: If Assumption 1–3 are satisfied, then there exist positive constants ε^*, μ, such that for all $t \in [0, \infty)$, $\max\{\| x(0)\|, \| y(0)\|, \| u\|, \| \dot{u}\|\} \leqslant \mu$, and $\varepsilon \in (0, \varepsilon^*]$, the errors between solutions of original system (1) and (2) and its reduced-order model (5) and boundary-layer model (7) satisfy

$$x(t, \varepsilon) - \hat{x}(t) = O(\varepsilon), \tag{10}$$

$$z(t, \varepsilon) - h(\hat{x}(t), u(t)) - \hat{y}(t/\varepsilon) = O(\varepsilon), \tag{11}$$

where $\hat{x}(t)$ and $\hat{y}(\tau)$ are the solutions of reduced-order model (5) and boundary-layer model (7), respectively. Furthermore, for any given $T > 0$, there exists a positive constant $\varepsilon^{**} \leqslant \varepsilon^*$ such that for $t \in [T, \infty)$ and $\varepsilon < \varepsilon^{**}$, it follows that

$$z(t, \varepsilon) - h(\hat{x}(t), u(t)) = O(\varepsilon)\,. \tag{12}$$

Remark 2: Equation (11) means that when Assumptions 1 and 3 are satisfied, we can use $h + \hat{y}$ to accurately represent the solution of fast dynamics for $\varepsilon \in [0, \varepsilon^*]$ and bounded inputs. However, it requires solving the boundary-layer model. Further, (12) means that if $\varepsilon \leqslant \varepsilon^{**} < \varepsilon^*$, the solution of fast transient can be estimated by only $h(t, \hat{x}(t))$ after $T > 0$. This result significantly simplifies the order reduction.

Proof: From Assumption 2, we know that the solution of reduced-order model is bounded for bounded inputs. Therefore, we can expect that x is also bounded if $\| x - \hat{x}\| = O(\varepsilon)$. However, we cannot use this inequality since it has not been proven yet. Therefore, we exploit signal truncation as Lemma 1 to show that x is in a compact set. Then by Assumption 1, we have that the argument of $f(\boldsymbol{x}, \boldsymbol{z}, \boldsymbol{u}, \varepsilon)$ is compact. Since f is continuous, it follows that f is bounded, i.e. $|f| \leqslant k_0$, and $x(t)$ is Lipschitz.

Then using Assumptions 1, 3, and Lemma 9.8 in [16], we conclude that there exists a Lyapunov function $V_y(x, y, u)$ and positive constants $b_1, b_2, \ldots, b_6$ and ρ_0 satisfying

$$b_1 \| y\|^2 \leqslant V_y(\boldsymbol{x}, y, \boldsymbol{u}) \leqslant ; b_2 \| y\|^2\,, \tag{13}$$

$$\frac{\partial V_y}{\partial y} G(\boldsymbol{x}, y, \boldsymbol{u}, 0) \leqslant -b_3 \| y\|^2\,, \tag{14}$$

$$\| \frac{\partial V_y}{\partial y}\| \leqslant b_4 \| y\|; \quad \| \frac{\partial V_y}{\partial x}\| \leqslant b_5 \| y\|^2; \quad \| \frac{\partial V_y}{\partial u}\| \leqslant b_6 \| y\|^2, \tag{15}$$

for all $y \in \{\| y\| < \rho_0\}$ and all $(\boldsymbol{x}, \boldsymbol{u}) \in \mathbb{R}^n \times \mathbb{R}^p$.

To assess the accuracy of solutions of fast dynamics, we define the estimation error as

$$\sigma_y(\tau, \varepsilon) = y(\tau, \varepsilon) - \hat{y}(\tau)\,. \tag{16}$$

Differentiate both sides of (16) and abbreviate $x(t_0 + \varepsilon\tau, \varepsilon), y(\tau, \varepsilon), u(t_0 + \varepsilon\tau, \varepsilon), \sigma_y(\tau, \varepsilon)$ as x, y, u, σ_y, respectively, then we have

$$\begin{aligned} \frac{\partial \sigma_y}{\partial \tau} &= G(\boldsymbol{x}, y, \boldsymbol{u}, \varepsilon) - G(x_0, \hat{y}, u_0, 0) \\ &= G(\boldsymbol{x}, \sigma_y, \boldsymbol{u}, 0) + \Delta G, \end{aligned} \tag{17}$$

where $\Delta G = G(\boldsymbol{x}, y, \boldsymbol{u}, \varepsilon) - G(\boldsymbol{x}, \sigma_y, \boldsymbol{u}, 0) - G(x_0, \hat{y}, u_0, 0)$. Utilising the Lipschitz conditions of G and x, and the condition of Lemma 1, we have (see (18)) for some non-negative constants $a, k_i, i = 1, \ldots, 5$ and non-negative Lipschitz constants $l_j, j = 1, \ldots, 3$, where $k_5 = l_1 + k_1 \max\{l_3 k_4, l_2 + l_3 k_0\} \times \max\{1, 1/a\}$.

Equation (17) can be viewed as the perturbation of

$$\frac{\partial \sigma_y}{\partial \tau} = G(\boldsymbol{x}, \sigma_y, \boldsymbol{u}, 0)\,. \tag{19}$$

Using (13)–(15) and (18), the derivative of Lyapunov funtion $V_y(\boldsymbol{x}, \sigma, \boldsymbol{u})$ along the trajectories of (17) can be calculated as

$$\begin{aligned} \dot{V}_y &= \frac{\partial V_y}{\partial x} f + \frac{1}{\varepsilon} \cdot \frac{\partial V_y}{\partial \sigma_y}(G + \Delta G) + \frac{\partial V_y}{\partial u}\dot{u} \\ &\leqslant b_5 k_0 \| \sigma_y\|^2 - \frac{b_3}{\varepsilon} \| \sigma_y\|^2 + b_6 \mu \| \sigma_y\|^2 \\ &\quad + \frac{b_4}{\varepsilon} \| \sigma_y\| (k_2 \| \sigma_y\|^2 + k_1 k_3 \| \sigma_y\| \mathrm{e}^{-a\tau} + \varepsilon k_5) \\ &\leqslant -\frac{b_3}{2\varepsilon} \| \sigma_y\|^2 + \frac{b_4 k_1 k_3}{\varepsilon} \mathrm{e}^{-a\tau} \| \sigma_y\|^2 + b_4 k_5 \| \sigma_y\| \\ &\leqslant -\frac{2}{\varepsilon}(\xi_1 - \xi_2 \mathrm{e}^{-a\tau}) V_y + 2\xi_3 \sqrt{V_y}, \end{aligned} \tag{20}$$

for $0 < \varepsilon \leqslant \varepsilon^*$ and $\| \sigma_y\| \leqslant b_3/(4 b_4 k_2)$, where $\xi_1 = b_3/(4 b_2)$, $\xi_2 = b_4 k_1 k_3/(2 b_1)$, $\xi_3 = b_4 k_5/(2\sqrt{b_1})$, and $\varepsilon^* = b_3/(b_5 k_0 + b_6 \mu)$.

Let $W_y = \sqrt{V_y}$ and use the comparison lemma, we have

$$W_y(\tau) \leqslant \phi(\tau, 0) W_y(0) + \varepsilon \xi_3 \int_0^\tau \phi(\tau, s) \quad \mathrm{d}s, \tag{21}$$

$$|\phi(\tau, s)| = \left|\mathrm{e}^{-\int_s^\tau (\xi_1 - \xi_2 \mathrm{e}^{-a v})\, dv}\right| \leqslant \xi_4 \mathrm{e}^{-\bar{a}(\tau - s)}, \tag{22}$$

for some positive constants ξ_4 and $\bar{a}$. Since $\sigma_y(0) = O(\varepsilon)$, it follows that $\sigma_y(\tau) = O(\varepsilon)$ for all $\tau \geqslant 0$. Then we can conclude that (11) holds $\forall \varepsilon \leqslant \varepsilon^*$ and $\forall\, t \geqslant 0$.

Moreover, from (9), we have $\mathrm{e}^{-at/\varepsilon} \leqslant \varepsilon$, $\forall\, at \geqslant \varepsilon \ln(1/\varepsilon)$, then the term $\hat{y}(t/\varepsilon)$ will be $O(\varepsilon)$ on $[T, \infty)$ for $\varepsilon \in [0, \varepsilon^{**}]$, where (ε^{**}, T) is a pair of solution of

$$\varepsilon \ln\left(\frac{1}{\varepsilon}\right) = aT\,. \tag{23}$$

$$\begin{aligned} \| \Delta G\| &\leqslant k_2 \| \sigma_y\|^2 + \varepsilon l_1 + (k_3 \| \sigma_y\| + l_2 |u - u_0| + l_3 \| x - x_0\|) \| \hat{y}\| \\ &\leqslant k_2 \| \sigma_y\|^2 + k_1 k_3 \| \sigma_y\| \mathrm{e}^{-a\tau} + \varepsilon l_1 + \varepsilon(l_2 \mu \tau + l_3 k_4 + l_3 k_0 \tau)\mathrm{e}^{-a\tau} \\ &\leqslant k_2 \| \sigma_y\|^2 + k_1 k_3 \| \sigma_y\| \mathrm{e}^{-a\tau} + \varepsilon k_5, \end{aligned} \tag{18}$$

1: Find the perturbation coefficients ε. Identify the states with ε as fast states, while the others as slow states.
2: **procedure** REDUCED MODEL DERIVATION
3: Let $\varepsilon = 0$, solve the algebraic equation (3) to obtain the isolated QSS solutions $z = h(x, u)$.
4: Substitute z into (1) to obtain reduced-order model (5)
5: Derive the boundary-layer model using equation (7).
6: **end procedure**
7: **procedure** CALCULATE THE BOUND OF ε
8: Calculate $\varepsilon^* = b_3/(b_5k_0+b_6\mu)$.
9: Calculate ε^{**} by solving equation (23).
10: **end procedure**
11: **procedure** ACCURACY ASSESSMENT
12: **if** $\varepsilon \leqslant \varepsilon^*$ **then**
13: **if** $\varepsilon \leqslant \varepsilon^{**}$ **then**
14: $z = h(\hat{x}, u)$ is the solution of fast dynamics
15: **else**
16: Use $z = h(\hat{x}, u) + \hat{y}$ by solving (7).
17: **end if**
18: **else**
19: Return to Step 1 to re-identify slow/fast dynamics
20: **end if**
21: **end procedure**

Fig. 2 *Algorithm 1: high-fidelity order reduction*

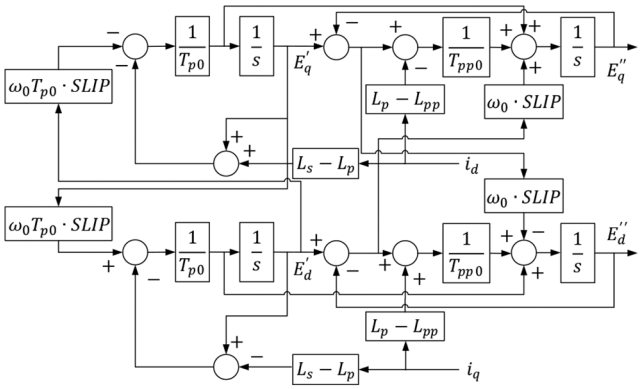

Fig. 3 *Block diagram of three-phase motor adopted in the WECC composite load model [14]*

Now we have proved the accuracy of the solutions of fast dynamics. To show the conditions for *accurate* solutions of slow dynamics, we can define $\sigma_x(t, \varepsilon) = x(t, \varepsilon) - \hat{x}(t)$. As (13)–(22), it can be verified that if Assumptions 1–3 are satisfied, then (10) holds for $\varepsilon \in [0, \varepsilon^*]$ and all $t \in [0, \infty)$. □

Remark 3: Note that ε^* is a function of the bound of input signals and it follows that

$$\lim_{\mu \to 0} \varepsilon^* = \frac{b_3}{b_5 k_0} \text{ and } \lim_{\mu \to +\infty} \varepsilon^* = 0. \tag{24}$$

This means when inputs are zero, the upper bound of ε is equal to that of its autonomous system; while when the inputs are unbounded, ε must be exactly zero to guarantee the accuracy of the reduced-order model. This result reflects the impact of external inputs on the accuracy of the reduced-order model.

The overall algorithm of this proposed high-fidelity order reduction method can be concluded as Algorithm 1 (see Fig. 2).

3 Mathematical representation of WECC composite load model

To apply the singular perturbation theory, we need the mathematical representation of WECC composite load model, which can be found in our previous work [20]. Since our objective is to reduce the order of *dynamic* parts, the static ones such as single-phase motor (which is modelled as a performance model [14]), electronic loads [2] and static load are out of the scope of this paper. For brevity, only the mathematical representation of dynamic components is introduced in this section.

3.1 Three-phase motor model

WECC composite load model uses three three-phase fifth-order IMs, called motors A, B, and C, to represent different types of dynamic components. These three-phase motors have the same structure but different parameter settings. The block diagram of the IM model is shown in Fig. 3. There are four dynamic equations with respect to E'_q, E'_d, E_q'', and E_d''. By adding the dynamic equation governing the slip s, we can represent the complete fifth-order model as follows:

$$\dot{E}'_q = \frac{1}{T_{p0}}\left[-E'_q - i_d(L_s - L_p) - E'_d \cdot \omega_0 \cdot s \cdot T_{P0}\right], \tag{25}$$

$$\dot{E}'_d = \frac{1}{T_{p0}}\left[-E'_d + i_q(L_s - L_p) + E'_q \cdot \omega_0 \cdot s \cdot T_{P0}\right], \tag{26}$$

$$\dot{E}_q'' = \frac{T_{p0} - T_{pp0}}{T_{p0}T_{pp0}}E'_q - \frac{T_{pp0}(L_s - L_p) + T_{p0}(L_p - L_{pp})}{T_{p0}T_{pp0}}i_d - \frac{1}{T_{pp0}}E''_q - \omega_0 \cdot s \cdot E''_d, \tag{27}$$

$$\dot{E}_d'' = \frac{T_{p0} - T_{pp0}}{T_{p0}T_{pp0}}E'_d + \frac{T_{pp0}(L_s - L_p) + T_{p0}(L_p - L_{pp})}{T_{p0}T_{pp0}}i_q - \frac{1}{T_{pp0}}E''_d + \omega_0 \cdot s \cdot E''_q, \tag{28}$$

$$\dot{s} = -\frac{p \cdot E_d'' \cdot i_d + q \cdot E_q'' \cdot i_q - T_L}{2H}. \tag{29}$$

The algebraic equations are

$$T_L = T_{m0}\left(Aw^2 + Bw + C_0 + Dw^{Etrq}\right), \tag{30}$$

$$T_{m0} = pE_{d0}''i_{d0} + qE_{q0}''i_{q0}, \tag{31}$$

$$w = 1 - s, \tag{32}$$

$$i_d = \frac{r_s}{r_s^2 + L_{pp}^2}(V_d + E_d'') + \frac{L_{pp}}{r_s^2 + L_{pp}^2}(V_q + E_q''), \tag{33}$$

$$i_q = \frac{r_s}{r_s^2 + L_{pp}^2}(V_q + E_q'') - \frac{L_{pp}}{r_s^2 + L_{pp}^2}(V_d + E_d''), \tag{34}$$

$$P = V_d i_d + V_q i_q, \tag{35}$$

$$Q = V_q i_d - V_d i_q, \tag{36}$$

where E'_q, E'_d, E_q'', E_d'', and s are the five state variables; L_s, L_p, and L_{pp} are synchronous reactance, transient, and subtransient reactance, respectively; T_{p0} and T_{pp0} are transient and subtransient rotor time constants, respectively; and ω_0 is the synchronous frequency.

3.2 DER_A model

Recently, EPRI developed a new model to represent aggregated renewable energy resources named DER_A which has fewer states and parameters than the previous PVD1 model. The block diagram of DER_A is shown in Fig. 4 and the dynamic model is as follows:

$$\dot{S}_0 = \frac{1}{T_{rv}}(V_t - S_0), \tag{37}$$

$$\dot{S}_1 = \frac{1}{T_p}(S_8 - S_1), \tag{38}$$

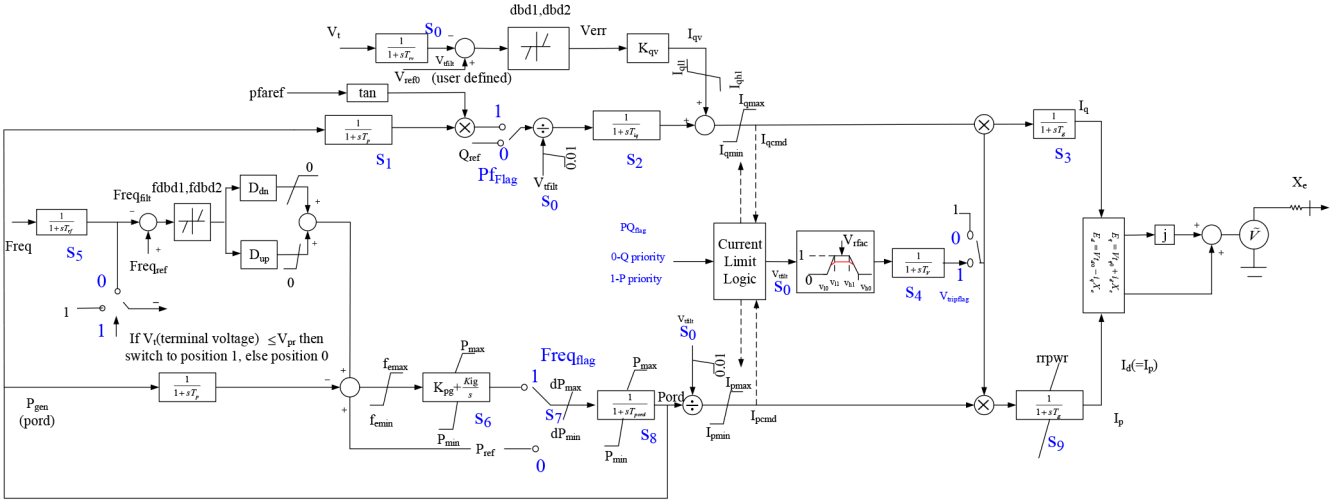

Fig. 4 *Block diagram of DER_A in the WECC composite load model developed by [15]*

$$\dot{S}_2 = \begin{cases} -\dfrac{S_2}{T_{iq}} + \dfrac{Q_{ref}}{T_{iq}\cdot \mathrm{sat}_1(S_0)} \text{if } \mathrm{Pf}_{flag} = 0, \\ -\dfrac{S_2}{T_{iq}} + \dfrac{\tan(\mathrm{pfaref})\times S_1}{T_{iq}\cdot \mathrm{sat}_1(S_0)} \text{if } \mathrm{Pf}_{flag} = 1, \end{cases} \tag{39}$$

$$\dot{S}_3 = \begin{cases} \dfrac{\mathrm{sat}_2\{S_2 + \mathrm{sat}_3[DB_V(V_{ref0} - S_0)\cdot K_{qv}]\} - S_3}{T_g} \\ \text{if } V_{tripflag} = 0, \\ \dfrac{\mathrm{sat}_2\{S_2 + \mathrm{sat}_3[DB_V(V_{ref0} - S_0)\cdot K_{qv}]\}\cdot S_4 - S_3}{T_g} \\ \text{if } V_{tripflag} = 1, \end{cases} \tag{40}$$

$$\dot{S}_4 = \frac{1}{T_v}(VP(S_0, V_{rfrac}) - S_4), \tag{41}$$

$$\dot{S}_5 = \frac{1}{T_{rf}}(\mathrm{Freq} - S_5), \tag{42}$$

$$\begin{aligned} \dot{S}_6 = K_{ig}\mathrm{sat}_4\{P_{ref} - S_1 + \mathrm{sat}_5[D_{dn}\cdot DB_F(\mathrm{Freq}_{ref} - S_5)] \\ + \mathrm{sat}_6[D_{up}\cdot DB_F(\mathrm{Freq}_{ref} - S_5)]\} + \frac{K_{pg}}{T_p}S_1 \\ + G_{dn}(\mathrm{Freq} - S_5) + G_{up}(\mathrm{Freq} - S_5) - \frac{S_8}{T_p}, \end{aligned} \tag{43}$$

$$\dot{S}_7 = \begin{cases} 0 & \text{if } \mathrm{Freq}_{flag} = 0, \\ \mathrm{sat}_8[\dot{\mathrm{sat}}_7(S_6)] & \text{if } \mathrm{Freq}_{flag} = 1, \end{cases} \tag{44}$$

$$\dot{S}_8 = \frac{1}{T_{pord}}(S_7 - S_8), \tag{45}$$

$$\dot{S}_9 = \begin{cases} \dfrac{1}{T_g}\left\{\mathrm{sat}_9\left[\dfrac{\mathrm{sat}_7(S_8)}{\mathrm{sat}_1(S_0)}\right]\times S_4 - S_9\right\} \text{if } V_{tripflag} = 1, \\ \dfrac{1}{T_g}\left\{\mathrm{sat}_9\left[\dfrac{\mathrm{sat}_7(S_8)}{\mathrm{sat}_1(S_0)}\right] - S_9\right\} \text{if } V_{tripflag} = 0, \end{cases} \tag{46}$$

where $\mathrm{sat}_i(x), i = 1, \ldots, 9$ are the saturation functions; $DB_V(x)$ and $DB_F(x)$ are deadzone functions with respect to voltage and frequency, respectively; and $VP(x, V_{rfrac})$ represents the voltage protection function, which is a piece-wise algebraic function. The parameter definitions are given in Table 1. Here we only summarise the dynamic equations that will be used in the order reduction. The complete detailed mathematical model can be found in [20].

4 Reduced-order WECC composite load model

In this section, we will derive the reduced-order large-signal model of WECC composite load model using singular perturbation method. For the purpose of order reduction, we only focus on the dynamic components. These components are connected in parallel and we will reduce each individual component's order.

4.1 Reduced-order three-phase motors model

Each three-phase motor model has five states, $\tilde{x}_M = [E'_q, E'_d, E''_q, E''_d, s]$. When applying Algorithm 1 (Fig. 2), the first step is to identify the slow and fast dynamics. Since the fast dynamics are characterised by the small perturbation coefficient ϵ, we rewrite the left-hand-side of the dynamic equations as

$$\left[T_{p0}\dot{E}'_q,\ T_{p0}\dot{E}'_d,\ T_{pp0}\dot{E}''_q,\ T_{pp0}\dot{E}''_d,\ H\dot{s}\right]^T. \tag{47}$$

Given one set of parameter setting in Table 2, (47) becomes

$$\left[0.1\dot{E}'_q, 0.1\dot{E}'_d, 0.0026\dot{E}''_q, 0.0026\dot{E}''_d, 0.1\dot{s}\right]^T. \tag{48}$$

The smaller perturbation coefficients in (48) suggest that dynamic response velocities of $[E'_q, E'_d, s]^T$ are much slower than the rest of the states. This difference is also an evidence of the two-time-scale property of this model. Then the slow and fast dynamics are divided as $\dot{\tilde{x}}_M = [\dot{x}_M, \dot{z}_M]^T$, where $x_M = [E'_q, E'_d, s]^T$, $z_M = [E''_q, E''_d]^T$. For consistency, denote the input voltages $[V_q, V_d]^T$ as U_M. Following the singular perturbation method (1)–(5), we can obtain the reduced-order large-signal model of three-phase motor as

$$\dot{x}_{M1} = \frac{1}{T_{p0}}\left[-x_{M1} - i_d(L_s - L_p) - \omega_0 T_{P0} x_{M2} x_{M3}\right], \tag{49}$$

$$\dot{x}_{M2} = \frac{1}{T_{p0}}\left[-x_{M2} + i_q(L_s - L_p) + \omega_0 T_{P0} x_{M1} x_{M3}\right], \tag{50}$$

$$\dot{x}_{M3} = \frac{T_L - p\cdot h_2(x_M)\cdot i_d - q\cdot h_1(x_M)\cdot i_q}{2H}, \tag{51}$$

where the QSS solutions are

$$\begin{aligned} h_1(x_M) = \frac{1}{r_s^2 + L_p^2}\big[&(L_p L_{pp} + r_s^2)x_{M1} - (L_p - L_{pp})r_s x_{M2} \\ &-(L_p - L_{pp})L_p U_1 - (L_p - L_{pp})r_s U_2\big], \end{aligned} \tag{52}$$

$$\begin{aligned} h_2(x_M) = \frac{1}{r_s^2 + L_p^2}\big[&(L_p - L_{pp})r_s x_{M1} - (L_p L_{pp} + r_s^2)x_{M2} \\ &+(L_p - L_{pp})r_s U_1 - (L_p - L_{pp})L_p U_2\big]. \end{aligned} \tag{53}$$

Table 1 Parameter definition of DER_A model [15]

Parameter	Definition
T_{rv}	transducer time constant (s) for voltage measurement
T_p	transducer time constant (s)
T_{iq}	Q control time constant (s)
V_{ref0}	voltage reference set-point $> 0(pu)$
K_{qv}	proportional voltage control gain (pu/pu)
T_g	current control time constant (s)
Pf_{Flag}	0 – constant Q control, and 1 – constant power factor control
I_{max}	maximum converter current (pu)
dbd1	lower voltage deadband $\leqslant 0(pu)$
dbd2	upper voltage deadband $\geqslant 0(pu)$
T_v	time constant on the output of voltage/frequency cut-off
V_{l0}	voltage break-point for low voltage cut-out of inverters
V_{l1}	voltage break-point for low voltage cut-out of inverters
V_{h0}	voltage break-point for high voltage cut-out of inverters
V_{h1}	voltage break-point for high voltage cut-out of inverters
t_{vl0}	timer for V_{l0} point
t_{vl1}	timer for V_{l1} point
t_{vh0}	timer for V_{h0} point
t_{vh1}	timer for V_{h1} point
V_{rfrac}	fraction of device that recovers after voltage comes back to within $V_{l1} < V < V_{h1}$
T_{rf}	transducer time constant (s) for frequency measurement (must be $\geqslant 0.02$ s)
K_{pg}	active power control proportional gain
K_{ig}	active power control integral gain
D_{dn}	frequency control droop gain $\geqslant 0$ (down-side)
D_{up}	frequency control droop gain $\geqslant 0$ (up-side)
f_{emax}	frequency control maximum error $\geqslant 0(pu)$
f_{emin}	frequency control minimum error $\leqslant 0(pu)$
f_{dbd1}	lower frequency control deadband $\leqslant 0(pu)$
f_{dbd2}	upper frequency control deadband $\geqslant 0(pu)$
$Freq_{flag}$	0 – frequency control disabled, and 1 – enabled
P_{min}	minimum power (pu)
P_{max}	maximum power (pu)
T_{pord}	power order time constant (s)
dP_{min}	power ramp rate down $< 0(pu/s)$
dP_{max}	power ramp rate up $> 0(pu/s)$
$V_{tripflag}$	0 – voltage tripping disabled, 1 – enabled
I_{ql1}	minimum limit of reactive current injection, p.u.
I_{qh1}	maximum limit of reactive current injection, p.u.
X_e	source impedance reactive $> 0(\,pu)$
$F_{tripflag}$	0 – frequency tripping disabled, 1 – enabled
PQ_{flag}	0 – Q priority, 1 – P priority – current limit
typeflag	0 – the unit is a generator $I_{pmin} = 0$, 1 – the unit is a storage device and $I_{pmin} = -I_{pmax}$
V_{pr}	voltage below which frequency tripping is disabled

Denote $\bar{x}_{M3} = 1 - x_{M3}$. The other algebraic equations are

$$T_L = T_{m0}\left[A\ \bar{x}_{M3}^2 + B\ \bar{x}_{M3} + C_0 + D\ \bar{x}_{M3}^{Etrq}\right], \tag{54}$$

$$T_{m0} = p \cdot h_2(x_M) \cdot i_d + q \cdot h_1(x_M) \cdot i_q, \tag{55}$$

$$i_q = \frac{r_s}{r_s^2 + L_p^2}(U_{M1} + x_{M1}) - \frac{L_p}{r_s^2 + L_p^2}(U_{M2} + x_{M2}), \tag{56}$$

$$i_d = \frac{L_p}{r_s^2 + L_p^2}(U_{M1} + x_{M1}) + \frac{r_s}{r_s^2 + L_p^2}(U_{M2} + x_{M2}). \tag{57}$$

By solving (23), we can find a pair of solution $(T, \varepsilon^{**}) = (0.012, 0.035)$. Since $\varepsilon_M = 0.0026 < 0.035$, the solutions of fast dynamics $\hat{z}_M$ converge to $h(\hat{x}_M)$ exponentially fast within time 0.012 s which is short enough. Therefore, we can use only the QSS solution $h(\hat{x}_M)$ to represent the solution of fast dynamics.

4.2 Reduced-order DER_A model

The DER_A model has ten states in total, $\tilde{x}_D = [S_0, S_1, \ldots, S_9]^T$. Different from the three-phase motor model, due to the existence of switches such as Pf_{flag} and PQ_{flag}, the DER_A model is actually a switching system consisting of $2^6 = 64$ subsystems. Each subsystem is determined when the switches are fixed. Since these

Table 2 Parameter setting of three-phase motor model

Motor A		Motor B		Motor C	
r_{sA}	0.04	r_{sB}	0.03	r_{sC}	0.03
L_{sA}	1.8	L_{sB}	1.8	L_{sC}	1.8
L_{pA}	0.1	L_{pB}	0.16	L_{pC}	0.16
L_{ppA}	0.083	L_{ppB}	0.12	L_{ppC}	0.12
T_{poA}	0.092	T_{poB}	0.1	T_{poC}	0.1
T_{ppoA}	0.002	T_{ppoB}	0.0026	T_{ppoC}	0.0026
H_A	0.05	H_B	1	H_C	0.1
A_A	0	A_B	0	A_C	0
B_A	0	B_B	0	B_C	0
C_A	0	C_B	0	C_C	0
D_A	1	D_B	1	D_C	1
E_{trqA}	0	E_{trqB}	2	E_{trqC}	2
p_A	-1	p_B	-1	p_C	-1
q_A	-1	q_B	-1	q_C	-1
ω_{0A}	120π	ω_{0B}	120π	ω_{0C}	120π

switches are preset, we only need to derive the reduced-order model for each subsystem. For brevity, we give the reduced-order model for one of the subsystems to illustrate the model order reduction procedure. The reduced-order models for other subsystems can be obtained using the same method.

To find ε, we rewrite the dy namics as

$$\begin{bmatrix} T_{rv}\dot{S}_0, \\ T_p\dot{S}_1, \\ T_{iq}\dot{S}_2, \\ T_g\dot{S}_3, \\ T_v\dot{S}_4, \\ T_{rf}\dot{S}_5, \\ T_p \cdot T_{rf}\dot{S}_6,\ \dot{S}_7,\ T_{pord}\dot{S}_8,\ T_g\dot{S}_9 \end{bmatrix}^T \quad (58)$$

.

Given the parameter setting in Table 3, (58) becomes (see (59)) The smaller perturbation coefficients in (59) suggest that dynamic response velocities of $[S_0, S_1, S_5, S_7]^T$ are much slower than other states. This difference is also an evidence of the two-time-scale property of this model. Then the slow and fast dynamics are divided as $\dot{x}_D = [\dot{x}_D, \dot{z}_D]^T$, where $x_D = [S_0, S_1, S_5, S_7]^T$, $z_D = [S_2, S_3, S_4, S_6, S_8, S_9]^T$. Define the terminal voltage and frequency $[V_t, \text{Freq}]$ as U_D. Following the same procedure as above (1)–(5), we can derive the reduced-order large-signal model of DER_A as

$$\dot{x}_{D1} = \frac{1}{T_{rv}}(U_{D1} - x_{D1}), \quad (60)$$

$$\dot{x}_{D2} = \frac{1}{T_p}(x_{D4} - x_{D2}), \quad (61)$$

$$\dot{x}_{D3} = \frac{1}{T_{rf}}(U_{D2} - x_{D3}), \quad (62)$$

$$\dot{x}_{D4} = 0\,. \quad (63)$$

To obtain the output power, we also need to calculate the output currents, which are identified as fast states. According to Algorithm 1 (Fig. 2), there are two options to represent the solutions of fast dynamics depending on the magnitude of ε. For simplicity, it it better to use only the QSS solution to represent the fast states since it does not require solving the boundary-layer model. Let $\varepsilon^{**} = 0.06$ to make sure max $\{\varepsilon_D\} < \varepsilon^{**}$, then solving (23), we obtain $T = 0.242$ s. This means if we use only the QSS solutions, the solution of fast dynamics is inaccurate within 0.242 s. This time period is intolerably long for stability analysis. Therefore, we should use $z = h + \hat{y}$ by solving the boundary-layer model. The d–q axis currents i_d and i_q are states S_3 (z_{D2}) and S_9 (z_{D6}), respectively. Their equations are

$$i_q = \text{sat}_2\{\gamma(x_D)\} \times VP(x_{D1}, V_{rfrac}) + \hat{y}_{D2}, \quad (64)$$

$$i_d = \text{sat}_9\left[\frac{\text{sat}_7(x_{D4})}{\text{sat}_1(x_{D1})}\right] \times VP(x_{D1}, V_{rfrac}) + \hat{y}_{D6}, \quad (65)$$

$$\gamma(x_D) = \frac{\tan(\text{pfaref})x_{D2}}{\text{sat}_1(x_{D1})} + K_{qv}\text{sat}_3[DB_V(V_{ref0} - x_{D1})], \quad (66)$$

where $\hat{y}_{D2}$ and $\hat{y}_{D6}$ are the solutions of boundary-layer model

$$\dot{y}_{D1} = -y_{D1}, \quad (67)$$

$$\begin{aligned} \dot{y}_{D2} &= y_{D3} - y_{D2} - VP(x_{D1}, V_{rfrac}) \times \\ &\{\text{sat}_2[\gamma(x_D)] + \text{sat}_2\,[y_{D1} + \gamma(x_D)]\}, \\ \dot{y}_{D3} &= -y_{D3}, \end{aligned} \quad (68)$$

$$\dot{y}_{D4} = -T_{rf}y_{D5}, \quad (69)$$

$$\dot{y}_{D5} = -y_{D5}, \quad (70)$$

$$\dot{y}_{D6} = -\text{sat}_9\left[\frac{\text{sat}_7(x_{D4})}{\text{sat}_1(x_{D1})}\right] - y_{D6} \times VP(x_{D1}, V_{rfrac}) \quad (71)$$

$$+\text{sat}_9\left[\frac{\text{sat}_7(y_{D5} + x_{D4})}{\text{sat}_1(x_{D1})}\right] \times [y_{D3} + VP(x_{D1}, V_{rfrac})]\,. \quad (72)$$

5 Model validation via simulation

In this section, the reduced-order models of three-phase motors and DER_A are tested in Matlab using different solvers. We compare the performance of reduced-order model with original model to verify the effectiveness of the proposed high-fidelity order reduction approach. Moreover, we compare the computational time

$$\left[0.1\dot{S}_0,\ 0.1\dot{S}_1,\ 0.005\dot{S}_2,\ 0.005\dot{S}_3,\ 0.005\dot{S}_4, 0.1\dot{S}_5,\ 0.1 \cdot 0.1\dot{S}_6,\ \dot{S}_7,\ 0.005\dot{S}_8,\ 0.005\dot{S}_9\right]^T. \quad (59)$$

Table 3 Parameter setting of DER_A model (base: 12.47 kV and 15.0 MVA)

Parameters	Values	Parameters	Values
T_{rv}	0.1 s	T_p	0.1 s
T_{iq}	0.005 s	V_{ref0}	0 pu
K_{qv}	5 pu/pu	T_g	0.005 s
Pf_{flag}	1	I_{max}	1.2 pu
dbd1	−0.05 pu	dbd2	0.05 pu
T_v	0.005 s	V_{l0}	0.44 pu
V_{l1}	0.49 pu	V_{h0}	1.2 pu
V_{h1}	1.15 pu	t_{vl0}	0.16 s
t_{vl1}	0.16 s	t_{vh0}	0.16 s
t_{vh1}	0.16 s	V_{rfrac}	0.7
T_{rf}	0.1 s	K_{pg}	0.1 pu
K_{ig}	10 pu	D_{dn}	20 pu
D_{up}	0 pu	f_{emax}	99 pu
f_{emin}	−99 pu	f_{dbd1}	−0.0006
f_{dbd2}	0.0006	$Freq_{flag}$	0
P_{min}	0 pu	P_{max}	1.1 pu
T_{pord}	0.005 s	dP_{min}	−0.5 pu/s
dP_{max}	0.5 pu/s	$V_{tripflag}$	1
I_{ql1}	−1 pu	I_{qh1}	1 pu
X_e	0.25 pu	$F_{tripflag}$	1
PQ_{flag}	0	typeflag	1
V_{pr}	0.8 pu	*a*	0.8 pu
b	5 s	*c*	1 s
d	0.9 pu		

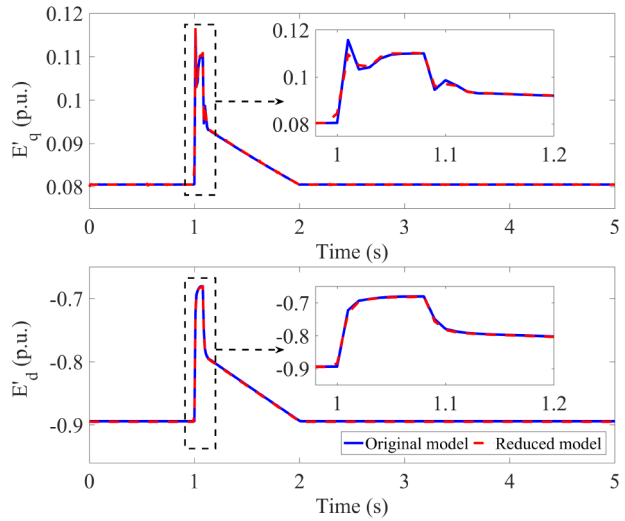

Fig. 5 *Dynamic responses of E'_d and E'_q of reduced/original models of three-phase motor A*

between two models using different solvers to show the reduction of computational burden.

5.1 Validation of reduced-order three-phase motors

To verify the proposed reduced-order model of three-phase motor, we simulate the reduced and original model in Matlab with the same input voltage. Consequently, we can compare their output power and other states. Refer to an EPRI white paper [15, 21], this paper tests a voltage sag benchmarking bus voltage input that is generated by (73). The parameters are set as Table 2 referring to [22].

$$V(t)=\begin{cases} a & \text{if } 1 \leqslant t < (1+b/60) \\ \dfrac{(1-d)(t-1-c)}{b/60-c}+1 & \text{if } (1+b/60) \leqslant t < 1+c \\ 1 & \text{otherwise} \end{cases} \quad (73)$$

Figs. 5–7 show the state responses of E'_q and E'_d for three-phase motors A, B and C, respectively. The blue solid lines denote E'_q and E'_d of the original model, while the red dashed lines represent those of the reduced-order model. Figs. 8–10 show the output real and reactive powers. The blue solid lines denote the real and reactive power of the original model, while the red dashed lines represent those of the reduced-order model. The mean squared errors of real and reactive power between the original and reduced-order model are shown in Table 4. The small errors show the accuracy of the proposed reduced-order three-phase model. Moreover, if using ODE45, which is a solver for non-stiff ODE problems, the computational time of the original and reduced-order model are 8.8120 and 0.1926 s, respectively. If using ODE15 s, which is a stiff ODE solver, the computational time of the original and reduced model are 1.0975 and 0.1785 s, respectively. This comparison shows that the singular perturbation method converts the original high-order stiff problem to a reduced-order non-stiff problem while considerably reducing the computational time. This reduction will be more significant in large-scale system with multiple composite loads.

5.2 Validation of DER_A model

Similar to the verification of three-phase motor, we simulate the original and reduced-order model of DER_A in Matlab. The voltage input is the same as (73). The frequency input is set to be 60 Hz. The parameter setting follows the reliability guideline in [23] as Table 3.

Fig. 11 shows the dynamic responses of DER_A. The blue lines denote the output powers of original model, while the red lines represent those of reduced one. Fig. 12 shows filtered voltage V_{tfilt}, filtered generated power $P_{genfilt}$, and filtered current i_q and i_d of reduced and original model of DER_A. The mean square errors

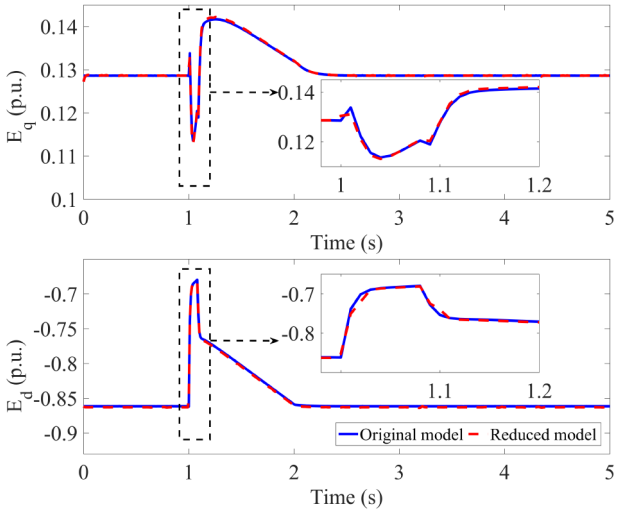

Fig. 6 *Dynamic responses of E'_d and E'_q of reduced/original models of three-phase motor B*

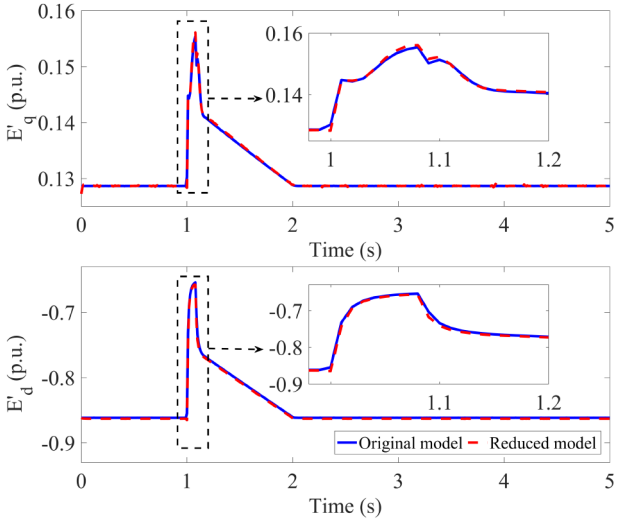

Fig. 7 *Dynamic responses of E'_d and E'_q of reduced/original models of three-phase motor C*

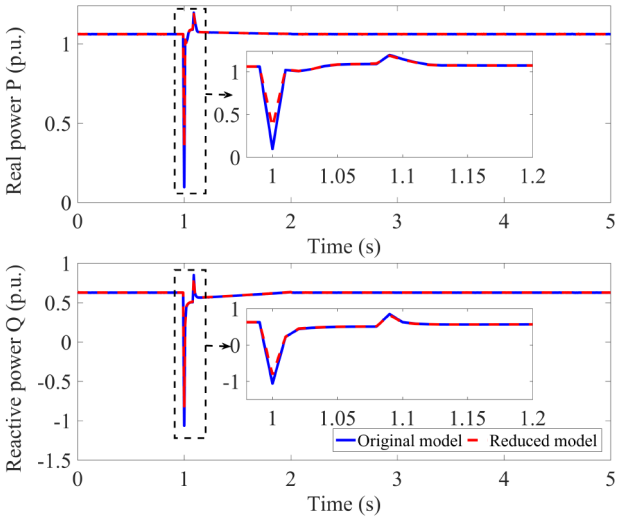

Fig. 8 *Real/reactive powers of reduced/original models of three-phase motor A*

(MSEs) of real and reactive power are 7.1363×10^{-4} and 1.3045×10^{-5}, respectively. Further, the computational time of original and reduced-order model using ODE45 are 11.205 and 0.2074 s, respectively; the computational time of original and

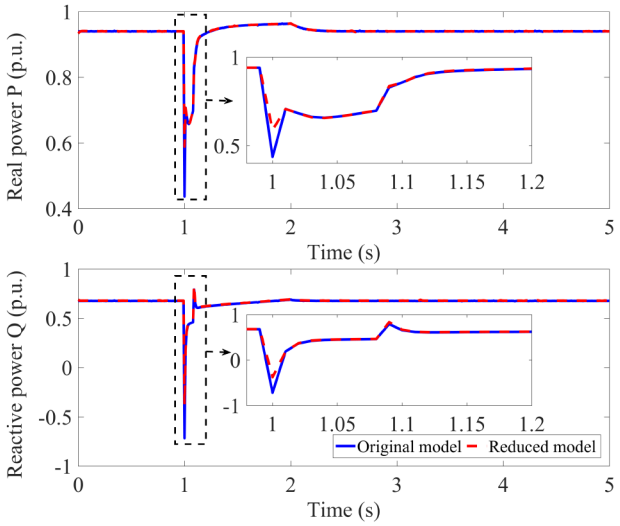

Fig. 9 *Real/reactive powers of reduced/original models of three-phase motor B*

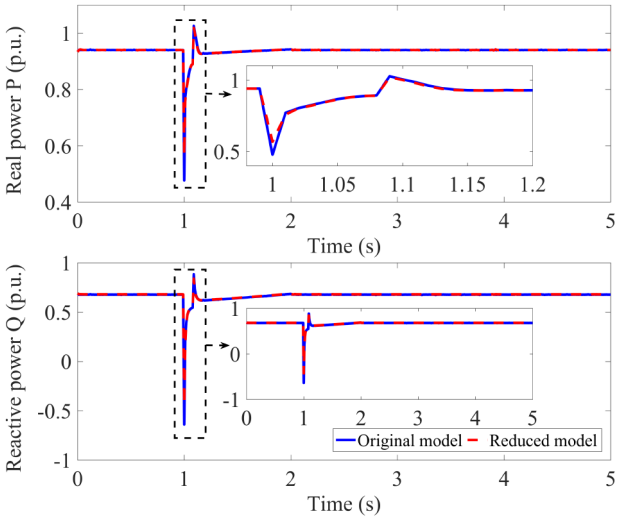

Fig. 10 *Real/reactive powers of reduced/original models of three-phase motor C*

Table 4 Mean squared errors between original and reduced-order model of three-phase motor

Power motor	Mean squared error		
	Motor A	Motor B	Motor C
real power	1.0509×10^{-4}	1.1295×10^{-4}	8.0264×10^{-5}
reactive power	1.1422×10^{-5}	1.4294×10^{-5}	2.1112×10^{-5}

reduced-order model using ODE15s are 2.0012 and 0.1598 s, respectively.

6 Conclusion

Q3 This paper proposes a high-fidelity LSOR approach for the latest WECC composite load model including DER_A. The derived reduced-order model has guaranteed high accuracy that can replace the original load model in high-order system simulation to perform power system studies. This replacement can significantly reduce the difficulty of stability analysis and computational burden. The simulation results verify the accuracy and efficiency of the proposed algorithm.

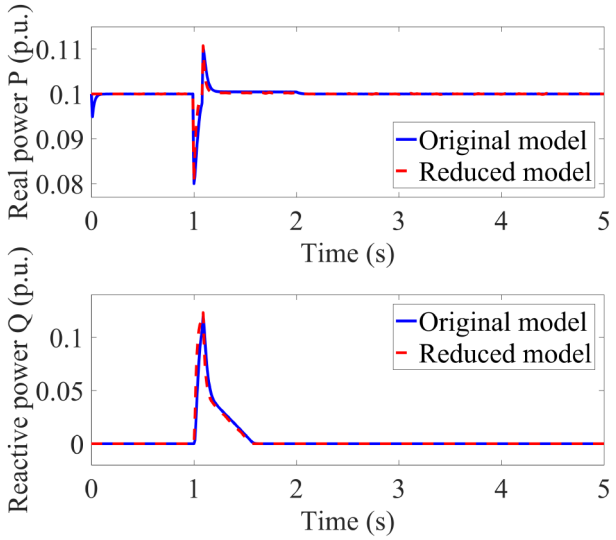

Fig. 11 *Real and reactive power of reduced and original model of DER_A*

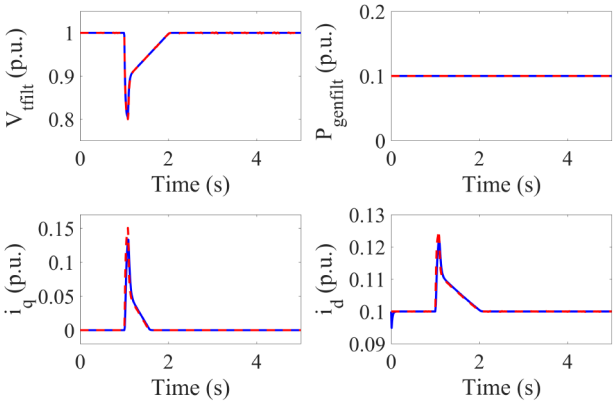

Fig. 12 *Filtered voltage V_{tfilt}, filtered generated power $P_{genfilt}$, and filtered current i_q and i_d of reduced and original model of DER_A*

7 References

[1] Taylor, C.W.: '*Power system voltage stability*' (McGraw-Hill, New York, 1994)

[2] Wang, C., Wang, Z., Wang, J., *et al.*: 'SVM-based parameter identification for composite ZIP and electronic load modeling', *IEEE Trans. Power Syst.*, 2019, **34**, (1), pp. 182–193

[3] Zhao, J., Wang, Z., Wang, J.: 'Robust time-varying load modeling for conservation voltage reduction assessment', *IEEE Trans. Smart Grid*, 2018, **9**, (4), pp. 3304–3312

[4] Kosterev, D., Meklin, A., Undrill, J., *et al.*: 'Load modeling in power system studies: WECC progress update'. Proc. IEEE Power and Energy Society General Meeting - Conversion and Delivery of Electrical Energy in the 21st Century, 2008, pp. 1–8

Q4 [5] Wang, C., Wang, Z., Wang, J., *et al.*: 'Robust time-varying parameter identification for composite load modeling', *IEEE Trans. Smart Grid*, 2019, **10**, (1), pp. 967–979

[6] Wang, J., Rhode-Barbarigos, W., Zuo, L., *et al.*: 'Literature review on modeling and simulation of energy infrastructures from a resilience perspective', *Reliab. Eng. Syst. Saf.*, 2019, **183**, pp. 360–373

Q5 [7] Zhang, K., Zhu, H., Guo, S.: 'Dependency analysis and improved parameter estimation for dynamic composite load modeling', *IEEE Trans. Power Syst.*, 2016, **32**, (4), pp. 3287–3297

[8] Guo, S., Shetye, K.S., Overbye, T.J., *et al.*: 'Impact of measurement selection on load model parameter estimation'. 2017 IEEE Power and Energy Conf. at Illinois (PECI). IEEE, 2017, pp. 1–6

[9] Cui, M., Wang, J., Wang, Y., *et al.*: 'Robust time-varying synthesis load modeling in distribution networks considering voltage disturbances', *IEEE Trans. Power Syst.*, 2019, **34**, (6), pp. 1–1

[10] Fu, C., Yu, Z., Shi, D., *et al.*: 'Bayesian estimation based parameter estimation for composite load', arXiv preprint 2019, arXiv: 1903.10695

[11] Kosterev, D.N., Taylor, C.W., Mittelstadt, W.A.: 'Model validation for the August 10, 1996 WSCC system outage', *IEEE Trans. Power Syst.*, 1999, **14**, (3), pp. 967–979

[12] Arif, A., Wang, Z., Wang, J., *et al.*: 'Load modeling-a review', *IEEE Trans. Smart Grid*, 2018, **9**, (6), pp. 5986–5999

[13] W.E.C. Council: 'WECC dynamic composite load model (CMPLDW) specifications', 2015

[14] Huang, Q., Huang, R., Palmer, B.J., *et al.*: 'A generic modeling and development approach for WECC composite load model', *Electr. Power Syst. Res.*, 2019, **172**, pp. 1–10

[15] Electrical Power Research Institute (EPRI): 'The new aggregated distributed energy resources (DER_A) model for transmission planning studies: 2019 update', 2019

[16] Khalil, H.K.: '*Nonlinear systems*' (Prentice Hall, New Jersey, 2000)

[17] Pekarek, S.D., Lemanski, M.T., Walters, E.A.: 'On the use of singular perturbations to neglect the dynamic saliency of synchronous machines', *IEEE Trans. Energy Convers.*, 2002, **17**, (3), pp. 385–391

[18] Rasheduzzaman, M., Mueller, J.A., Kimball, J.W.: 'Reduced-order small-signal model of microgrid systems', *IEEE Trans. Sustain. Energy*, 2015, **6**, (4), pp. 1292–1305

[19] FerreiradeJesus, R.M.G., Castro, J.M.: 'A wind park reduced-order model using singular perturbations theory', *IEEE Trans. Energy Convers.*, 1996, **11**, (4), pp. 735–741

[20] Ma, Z., Wang, Z., Wang, Y., *et al.*: 'Mathematical representation of the WECC composite load model', arXiv preprint, 2019, arXiv:1902.08866

[21] Electric Power Research Institute (EPRI): 'Distributed energy resources modeling for transmission planning studies. Summary modeling guidelines', 2016

[22] Wang, X., Wang, Y., Shi, D., *et al.*: 'Two-stage WECC composite load modeling: a double deep q-learning networks approach', *IEEE Trans. Smart Grid*, 2020, **11**, pp. 4331–4344, in press

Q6 [23] North American Electric Reliability Corporation (NERC): 'Reliability guideline-parameterization of the DER_A model', June 2019